Jung-Ting Tsai
School of Materials Engineering,
Purdue University,
West Lafayette, IN 47907
e-mail: tsai92@purdue.edu

Semih Akin
School of Mechanical Engineering,
Purdue University,
West Lafayette, IN 47907
e-mail: sakin@purdue.edu

Fengfeng Zhou
School of Mechanical Engineering,
Purdue University,
West Lafayette, IN 47907
e-mail: zhou966@purdue.edu

Min Soo Park
Department of Mechanical System Design Engineering,
Seoul National University of Science and Technology,
Seoul 01811, South Korea
e-mail: pminsoo@seoultech.ac.kr

David F. Bahr
School of Materials Engineering,
Purdue University,
West Lafayette, IN 47907
e-mail: dfbahr@purdue.edu

Martin Byung-Guk Jun[1]
School of Mechanical Engineering,
Purdue University,
West Lafayette, IN 47907
e-mail: mbgjun@purdue.edu

Electrically Conductive Metallized Polymers by Cold Spray and Co-Electroless Deposition

Conducting coatings on polymer substrates is of particular interest in sustainable electronics. Despite great promises, current approaches have significant limitations to producing conductive layers on polymers in a sustainable, large-scale, and high-throughput manner. This study hybridizes cold spray particle deposition with a co-electroless deposition (i.e., over-plating) process to achieve high-electrically conductive metallization on polymer surfaces. The resulting conducting polymer retains its intrinsic mechanical strength while providing multifunctional engineering performances. Numerical modeling and a series of characterizations are conducted to investigate both the cold-spraying process and the performance of resultant conductive coatings on polymers. Numerical simulations on high-velocity particle impact on the polymer (i.e., polyamide) surface provide useful information for optimum cold-spraying process parameters. The microstructure of as-sprayed and over-plated samples is thoroughly examined using scanning electronic microscopy. Cyclic voltammetry results reveal that the metallized polymers are stable after multiple cycles. The resultant electrodes through the hybrid metallization technique (i.e., cold spray coupled with over-plating) are highly conductive and stable, thereby having the potential for sustainable polymer electronics. [DOI: 10.1115/1.4053781]

Keywords: cold spray, finite element analysis, conductive coating, electroless deposition, polymer electronics, advanced materials and processing, coatings, manufacturing technology

1 Introduction

Conducting polymers attracts widespread interest in sustainable electronics applications owing to intrinsic advantages of polymers including high-impact resistance, lightweight, dimensional stability, and low cost. Current approaches to produce conducting coatings on polymers (i.e., electrically conductive polymer metallization) involve the use of either chemical vapor deposition, physical vapor deposition, screen-printing, ink-jet printing, or electroless deposition [1–5]. Despite great promises, these methods have significant limitations in producing conducting traces on polymers in a large-scale, high-throughput, eco-friendly, and facile manner.

Within the last decades, cold spray (CS) particle deposition has been successfully used in the metallization of various polymers, and promising results have been obtained [6–11]. In the CS deposition process, as shown in Fig. 1(*a*), microscale (5–60 μm) metal particles are accelerated to supersonic velocities using a converging–diverging nozzle and then impact a target surface. During the impact/impingement of the particles, the kinetic energy of particles dissipates over the substrate surface, resulting in a high-bond strength metal coating. Here, two deposition mechanisms are responsible for the CS coating process: (1) metallurgical bonding and (2) mechanical interlocking at particle–substrate interfaces [12]. In metallurgical bonding, the particles are plastically deformed on a harder substrate surface (e.g., cold spraying of copper (Cu) particles onto a steel substrate) under high-impact velocities due to adiabatic shear instabilities, resulting in high-strain rate and localized plastic deformation at particle–substrate interfaces [13]. Unlike metal substrates, particles do not significantly plastically deform when impinging upon the much softer polymeric surface [14]. Instead of plastic deformation, particles are mechanically interlocked (i.e., embedded) on the polymer surface, leading to a metallic layer after further deposition [15]. As such, CS particle deposition on polymer surfaces is mainly determined by the mechanical interlocking phenomenon.

Although CS particle deposition is a promising technology to achieve high-bond strength metallic coatings on polymer surfaces owing to the mechanical interlocking phenomena, the resulting coatings generally suffer from poor electrical conductivity. Substrate erosion [16] and local melting of polymer (i.e., wherein the polymer acts as a separator between the cold-sprayed particles) [14] are mainly responsible for the low-electrical conductivity. Although some researchers have attempted to solve this challenge by adjusting spray parameters for each spray pass, it remains challenging due to the possible damage to polymers' structural integrity [15,17,18].

Recently, over-plating processes of either electroplating or electroless plating have been proposed to modify the as-cold-sprayed layer in an electrically conductive manner [19,20]. In these methods, an as-cold sprayed layer on the polymer surface was utilized as the catalyst side (i.e., seed material) for a subsequent over-plating process. Most recently, our group hybridized the

[1]Corresponding author.

Manuscript received November 4, 2021; final manuscript received February 2, 2022; published online February 25, 2022. Assoc. Editor: Marcelo A. Trindade.

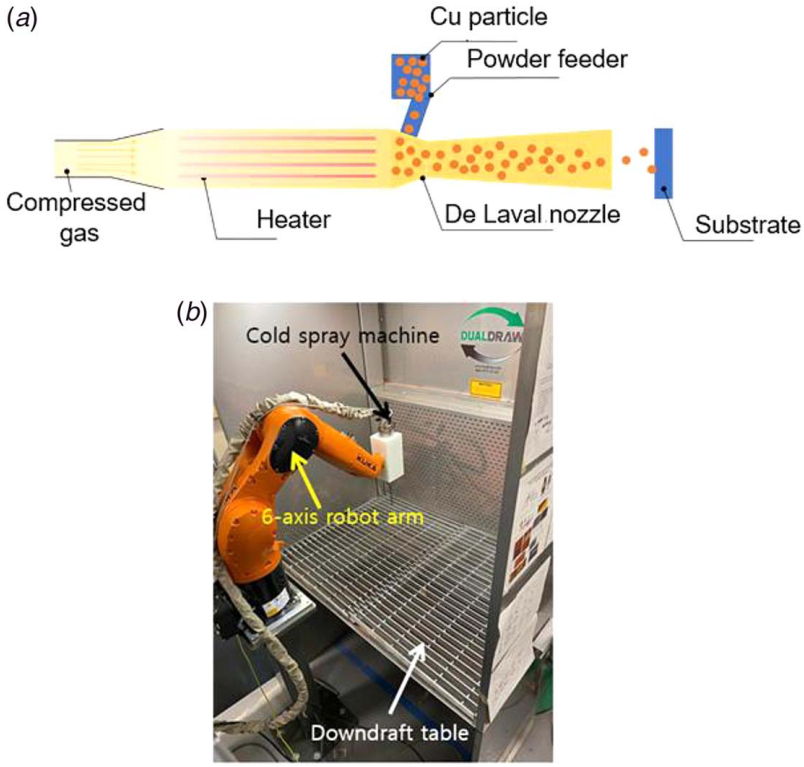

Fig. 1 (*a*) Schematic of a typical CS process and (*b*) experimental setup

cold-spraying process with a co-electroless deposition (co-ED) (i.e., over-plating) to obtain electrically conductive patterns on the acrylonitrile-butadiene-styrene (ABS) polymer surface [19]. The proposed hybrid surface coating approach enabled the electrically conductive metallization on the polymer surface in a manner that conductive patterns can be achieved selectively without the need of environmentally hazardous presurface treatments (e.g., acid etching, palladium absorption) that is often required in conventional electroless metallization methods on polymers [21,22].

Here, it is noteworthy that although electroless metallization leads to high-electrical conductivity (i.e., ≅ bulk resistivity of Cu), it does not solely guarantee high-adhesion strength metallization on the polymer surface. To increase the adhesion strength, electroless metallization generally requires presurface etching processes using strong acids [23]. On the other hand, cold spray ensures the high-bond strength coating without a need for presurface treatment owing to mechanical interlocking of the particles at the polymer interface, but the resulting cold spray coatings generally suffer from poor electrical conductivity due to the surface erosion and particles encapsulation by the polymer jetting (i.e., locally melting) [14]. As such, in our previous study [19], we hybridized the CS and electroless metallization to integrate the superior adhesion property of CS particle deposition and promising electrical conductivity of electroless over-plating to achieve high electrically conductive electrodes on polymer surfaces. In our previous study, however, the CS deposition mechanism and the effect of CS operational parameters on polymer metallization were not elucidated. These are integral to expanding cold-spray-based conductive metallization on polymers in a wide range of sustainable polymer electronics applications.

To this end, we attempt to fill this gap in the present study by systematically studying: (1) high-velocity cold spray particle impact by numerical modeling; (2) microstructure; (3) adhesion performance; (4) electrical conductivity; and (5) mechanical strength of the resultant metallic coatings. Besides, this study aims to uncover the process-structure properties of the described hybrid manufacturing approach for rapid and scalable production of conducting polymers in sustainable electronics.

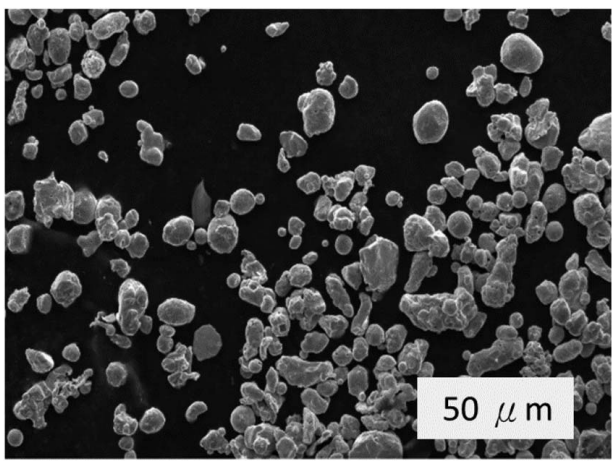

Fig. 2 Morphology of copper (Cu) particles

2 Materials and Methods

2.1 Materials. Microscale copper (Cu) particles were used as the CS feedstock material. The particles have quasi-spherical morphology having a circular equivalent average particle size of 5 μm (see Fig. 2). Polyamide, also known as Nylon 6, was used as the polymer substrate. The chemicals for the co-ED process were purchased from Sigma-Aldrich (St Louis, MO) and used without further purification. The chemicals and their associated mixing ratios to prepare the electroless plating bath are summarized in Sec. 2.4.

2.2 Cold Spray Particle Deposition. A low-pressure CS machine (Rus Sonic Technology, Inc., WA, US, Model no:

K205/407) was used in the particle deposition experiments. The CS nozzle was mounted on a six-axis robot arm to precisely control the coating process (see Fig. 1(*b*)). Microscale Cu particles were sprayed onto the polymer surface (i.e., polyamide) using the CS parameters listed in Table 1. The effect of CS parameters on particle deposition was further investigated by numerical modeling.

2.3 Numerical Modeling. This section describes the numerical modeling to capture the high-velocity impact of cold-sprayed particles. Simulation properties, boundary conditions, and material modeling are also explained in detail.

2.3.1 Simulation Properties. Finite element (FE) simulations considering the vertical impact of perfectly spherical Cu particles (i.e., having a diameter range of 5–40 μm) on a polyamide 6 substrate were conducted. Numerical simulations were performed using a commercially available FE analysis software ABAQUS/EXPLICIT 2018 equipped with PolyUMod®. A two-dimensional (2D) axisymmetric model was used to decrease the computational time. As the boundary conditions, the bottom of the substrate is fixed, and the symmetry boundary condition of the *x*-plane is applied along the *Y*-axis (see Fig. 3).

The Lagrangian numerical method was used in this research for a 2D surface impact to understand the energy transfer between the particles and the substrate. The trend would predict what cases the particles are likely to stick onto the substrate. The substrate dimension was assumed to be ten times the particle radius (i.e., 20 μm) to avoid the reflecting waves, which cause an excessive deformation by travelling back to the impact area. The general contact friction coefficient at the interface was set as 0.3 for each study. A unit mesh having a size of 0.02 μm was used for both particle and the substrate to achieve consistent results. A four-node bilinear plain strain quadrilateral element was used for both the particle and the substrate.

Table 1 Cold spray operating parameters

Operating parameter	Operating constants
Gas inlet pressure	0.5 MPa
Gas inlet temperature	298 K
Nozzle transverse speed	0.1 m/s
Nozzle standoff distance	10 mm

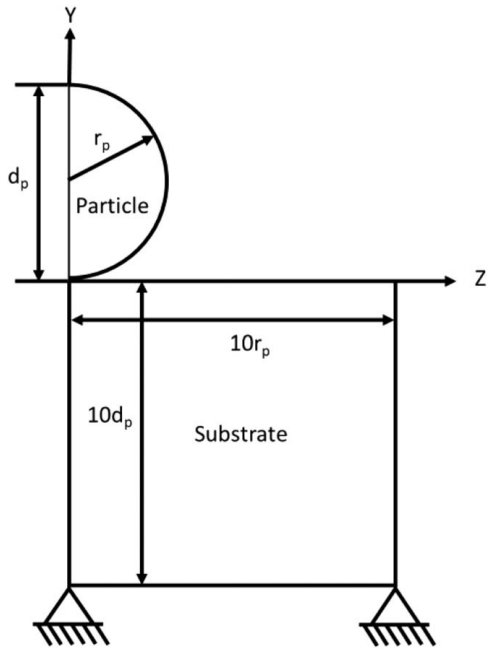

Fig. 3 Computational domain and boundary conditions

2.3.2 Material Models. The elastic region of the material was assumed to be linear for both Cu particle and the substrate. The Johnson–Cook (JC) plasticity model was used to simulate the particle impact on the substrate owing to its well-acceptance in the CS particle deposition [24–26]. The JC modeling as given in Eq. (1)

$$\sigma = [A + B\varepsilon^{n}][1 + C\ln\dot{\varepsilon}^{*}][1 - T^{*m}] \tag{1}$$

where A is the yield stress, B is the hardening constant, C is the strain rate constant, n is the hardening exponent, m is the thermal softening exponent, and T is the temperature. The corresponding material properties of the JC model are listed in Table 2.

The deformation of polyamide 6 substrates was simulated using an already developed three-network model consisting of parallelly acting three parts (i.e., molecular networks) [27]. The three parallel network models are stated as A, B, and C, respectively. More details and validation of this model can be found in Refs. [28–30]. We assumed that the material constants of the polymer do not vary during the impact of the particles. Note that, in this research, the model only considers the polymer plastic deformation at room temperature under the impact of cold-sprayed particles, assuming that the heat dissipation energy is in equilibrium. The model also neglects the long-range microstructural effects, which should be a possible limitation of the model to be improved as the future work. This model was developed explicitly for thermoplastic materials and described by the following equations:

$$\sigma_{\mathrm{A}} = \frac{\mu_{\mathrm{A}}}{J^{e}_{\mathrm{A}}\bar{\lambda}^{e^*}_{\mathrm{A}}} \times \frac{\mathcal{L}^{-1}\left(\frac{\bar{\lambda}^{e^*}_{\mathrm{A}}}{\lambda_{\mathrm{L}}}\right)}{\mathcal{L}^{-1}\left(\frac{1}{\lambda_{\mathrm{L}}}\right)} \times \mathrm{dev}[b^{e^*}_{\mathrm{A}}] + \kappa(J^{e}_{\mathrm{A}} - 1)I \tag{2}$$

$$\sigma_{\mathrm{B}} = \frac{\mu_{\mathrm{B}}}{J^{e}_{\mathrm{B}}\bar{\lambda}^{e^*}_{\mathrm{B}}} \times \frac{\mathcal{L}^{-1}\left(\frac{\bar{\lambda}^{e^*}_{\mathrm{B}}}{\lambda_{\mathrm{L}}}\right)}{\mathcal{L}^{-1}\left(\frac{1}{\lambda_{\mathrm{L}}}\right)} \times \mathrm{dev}[b^{e^*}_{\mathrm{B}}] + \kappa(J^{e}_{\mathrm{B}} - 1)I \tag{3}$$

$$\sigma_{\mathrm{C}} = \frac{\mu_{\mathrm{C}}}{J\,\lambda_{\mathrm{chain}}} \times \frac{\mathcal{L}^{-1}\left(\frac{\lambda_{\mathrm{chain}}}{\lambda_{L}}\right)}{\mathcal{L}^{-1}\left(\frac{1}{\lambda_{\mathrm{L}}}\right)} \times \mathrm{dev}[b^{e^*}] + \kappa(J - 1)I \tag{4}$$

where $J^{e}_{\mathrm{A}} = \det[F^{e}_{\mathrm{A}}]$, $b^{e^*}_{\mathrm{A}} = J^{e-2/3}_{\mathrm{A}} F^{e}_{\mathrm{A}}(F^{e}_{\mathrm{A}})^{T}$, $\bar{\lambda}^{e^*}_{\mathrm{A}} = (\mathrm{tr}[b^{e^*}_{\mathrm{A}}/3]^{1/2})$, $\mathcal{L}(x) = \coth(x) - 1/x\,\mu$, μ_{A}, and μ_{C} are the shear modulus of network A and network C, respectively. λ_L is the locking stretch, μ_{Bi} and μ_{Bf} are the initial and final shear modulus of network B, respectively and κ is the bulk modulus.

Table 2 Material constants of Johnson–Cook plasticity model

Material property	Material constant
Density, ρ (kg/m^3)	8.9×10^3
Shear modulus, G (GPa)	44.7
Yield stress, A (MPa)	90
Hardening constant, B (MPa)	292
Hardening exponent, n	0.31
Strain rate constant, C	0.025
Thermal softening exponent, m	1.09
Melting temperature, T_m (K)	1356
Reference temperature, T_o (K)	298

Table 3 Material constants of the three-network model for the polyamide polymer

Material property	Material constants
μ_A (MPa)	2350.68
λ_L (MPa)	7.52
κ (MPa)	3500
τ_A (MPa)	13
μ_A	7.63
μ_{Bi} (MPa)	547.26
μ_{Bf} (MPa)	154.32
B	12.08
τ_B (MPa)	65.75
μ_B	15.71
μ_C	1.62

The total results of the Cauchy stress tensor are described by the sum of the stresses in the three-network model. The material constants of the three-network model are also listed in Table 3. The material constants were taken from the experimental results of a Split-Hopkinson pressure bar test applied on a polyamide polymer substrate [31]. Note that the cold-sprayed particles impact a large area of polymer substrate (i.e., continuous bombarding); thus, in this research, the three-network model assumes that the polymer at the macroscale level is homogenized rather than at the local region where the molecular is disordered or amorphous.

2.4 Co-electroless Deposition (Over-plating). Following the CS particle deposition, the co-ED process (i.e., over-plating) was applied to obtain high-electrical conductivity on the polymer surface. Here, as-cold sprayed layer was utilized as the catalyst side for the subsequent co-ED process. As such, the polymer surface was functionalized as a conducting polymer. The electroless over-plating process was applied by following a published recipe [3]. The ingredient of the co-ED overcoating process is presented in Table 4. In the co-ED process, Cu sulfate is used as a Cu^+ source, ethylenediaminetetraacetic (EDTA) and hydrochloric acid (HCl) are complex agents, sodium hydroxide (NaOH) is the pH stabilizing agent, and potassium ferricyanide ($K_3[Fe(CN)_6$) is a stabilizing agent [3,32]. Lastly, formaldehyde (CH_2O) is the reducing agent that initiates the metal ion chemical deposition process. The samples were horizontally and evenly placed in the plating bath under continuous stirring. A set of co-ED times (i.e., 2, 4, 8, 16, and 24 h) was applied at room temperature to characterize the co-ED process. The over-plated samples were then rinsed with de-ionized (DI) water in the ultrasonic bath for 5 min.

Table 4 Chemical ingredients of the co-ED process

Content	Volume
Cu sulfate	18 (g/L)
EDTA	48 (g/L)
Sodium hydroxide	48 (g/L)
Hydrochloric acid	18 (mL/L)
Potassium ferricyanide	0.05 (g/L)
DI water	1 (L/L)
Formaldehyde	15 (mL/L)

3 Results and Discussion

3.1 Cold Spray Particle Impact. The simulation results of high-velocity CS particle impact on the polymer surface are shown in Figs. 4(*a*)–4(*c*). Herein, the initial particle velocity was set to 50 m/s, 150 m/s, and 300 m/s, while the particle size diameter was 40 μm for all testing conditions. The initial particle velocity was applied between 50 m/s and 300 m/s, considering that the cold spray system's input air pressure ranges from 0.5 MPa to 0.7 MPa. Our previous study has correlated the particles' velocity for the same pressure range using a dual disc anemometer to capture the particles' impact velocity [28]. The characterization of particle impact velocity at different gas pressures indicated that an increase in the gas inlet pressure leads to higher particles' impact

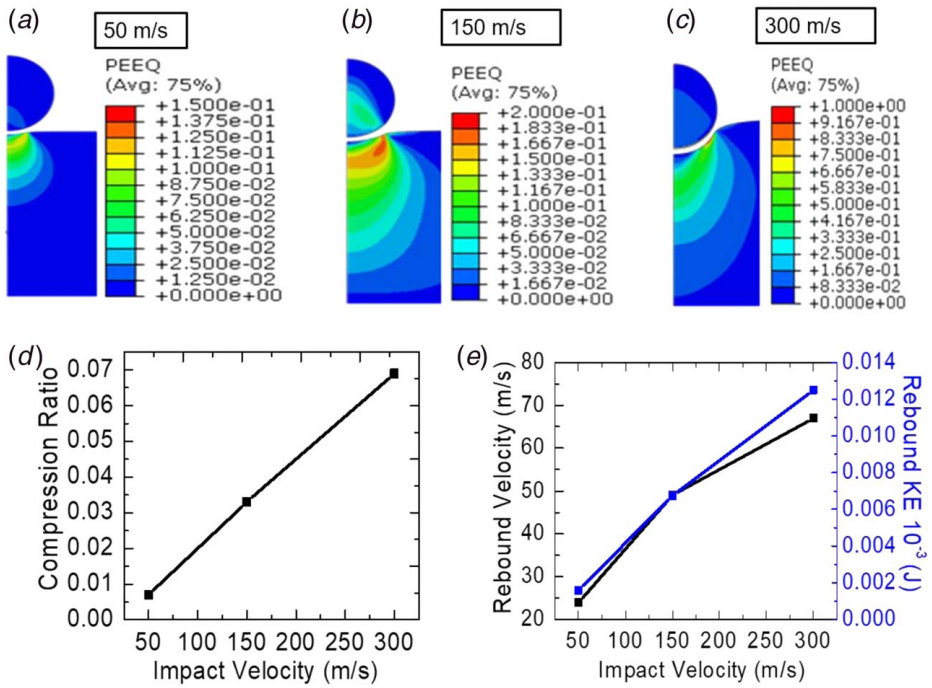

Fig. 4 Simulation results of single Cu particle (40 μm) impacting on the polymer surface at an impact velocity of (*a*) 50 m/s, (*b*) 150 m/s, (*c*) 300 m/s, (*d*) Cu particle compression ratio after a rebound for different impact velocities, and (*e*) rebound velocity and kinetic energy variation against particle impact velocity

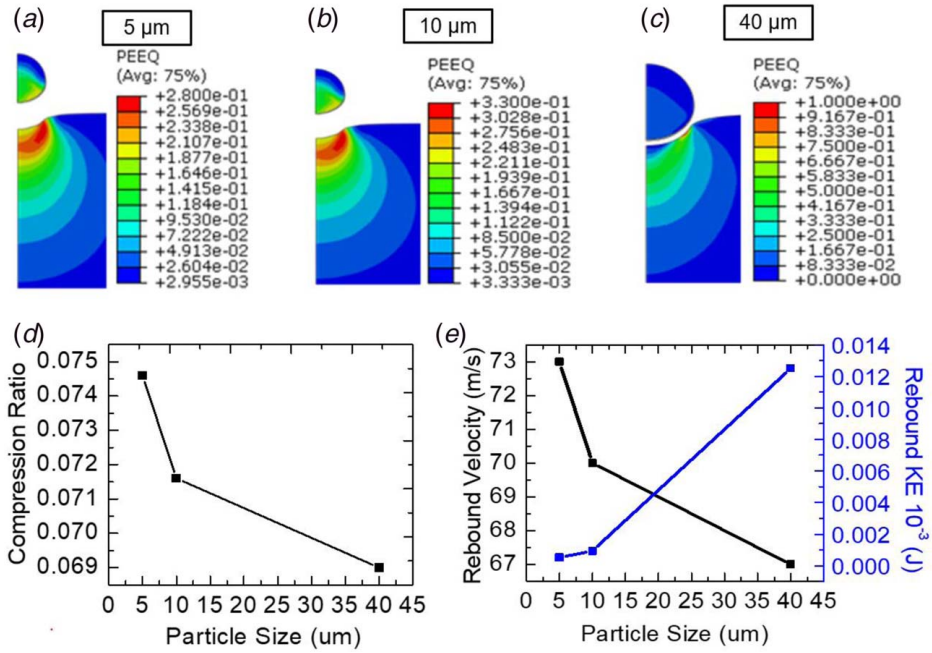

Fig. 5 Simulation results of different-size single Cu particle impacting on the polymer surface at a constant impact velocity of 300 m/s: (*a*) 5 μm, (*b*) 10 μm, (c) 40 μm, (*d*) Cu particle compression ratio after a rebound for different particle sizes, and (e) rebound velocity and kinetic energy variation against particle size

velocity that could be attributed to kinetic energy gain of the driving gas at higher pressures [28].

The compression ratio was taken from the original Cu shape and after impact. The maximum rebounding velocity value was calculated right before the particle separation from the polymer surface. The rebound kinetic energy value was calculated from the rebound velocity and a set of mass values (see Figs. 4(*d*) and 4(*e*)). The simulation results reveal that Cu particles impinge on the polymer substrate without deformation, unlike the cold spraying of metal particles on a metal substrate (e.g., Cu particle deposition on a stainless-steel substrate). The deposition of the particles on the polymer surface is attributed to mechanical interlocking, rather than metallurgical bonding due to polymers' intrinsic soft nature as compared to most of the metal substrate and particles. As such, polymers tend to plastically deform under the high impact of cold-sprayed particles, which results in embedding/impingement of the as-sprayed particles into the polymer surface. The results reveal that as the impact velocity increases, the Cu particle substantially impinges into the polymer substrate. In Fig. 4(*d*), the impact velocities are plotted against the Cu particle's compression ratio. After impact, the particle retained its original shape, and a lower rebound velocity was observed and compared to the impact velocities of 150 m/s and 300 m/s. The compression ratio of the Cu particle increases as the impact velocity rises (see Fig. 4(*d*)), resulting in severe deformation of the polymer substrate. Figure 4(*e*) shows the rebound velocity and the rebound kinetic energy against particle impact velocity. The results show that the rebound velocity and the rebound kinetic energy increase proportionally with an increasing impact velocity.

Figures 5(*a*)–5(*c*) show the different-size particle (i.e., 5, 10, and 40 μm) impact on the polymer surface at a constant impact velocity of 300 m/s. Simulation results suggested that Cu particles can impinge into a polymer substrate at an impact velocity of 300 m/s without the significant deformation of the Cu particle. This is likely attributed to polymer's soft nature (i.e., less rigidity) as compared to metal feedstock Cu particles. This phenomenon can also be observed in Fig. 6(*a*1), in which the as-sprayed Cu particles impinge to the polymer surface without significantly compromising particles' initial spherical shape. Furthermore, as shown in Fig. 5(*d*), the Cu particle compression ratio increases as the particle size decreases. This result suggests that smaller particles are more susceptible to deformation than larger particles at a constant impact velocity. It is likely attributed to the reduced contact area of smaller particles as compared to larger particles, which leads to more stress concentration during the contact of small particles with the polymer surface. Moreover, the rebound kinetic energy rises while the rebound velocity decreases with an increasing particle size (see Fig. 5(*e*)). Thus, smaller particles have less rebound kinetic energy and are unlikely to stick onto the polymer substrate. On the other hand, larger particles have higher kinetic energy due to their higher mass and they are inclined to attach to the polymer substrate. Taken together, the simulation results provided helpful information for the experimental cold-spraying and the subsequent co-ED process, which could be potentially used in CS metallization on polymer surfaces.

3.2 Microstructure Investigation. Figure 6 shows the top surface scanning electron microscopy (SEM) analysis of the as-sprayed polymer surface after 2 h, 4 h, 8 h, 16 h, and 24 h of the co-ED. The as-sprayed specimen shows the microscale particles attached to the polymer substrate, including microporosity and severe void formation (see Fig. 6(*a*)). In particular, Fig. 6(*a*1) (i.e., taken away from the concentrate cold spray coating area from Fig. 6(*a*)) shows single Cu particles embedded into the polymer substrate. When the co-ED process is introduced, the voids between the polymer base material and the Cu particles are filled. At 24 h co-ED, the surface was utterly over-plated with Cu particles, and no porosity on the surface was observed (see Fig. 6(*f*)). This result suggests that a subsequent over-plating process could help to overcome the severe erosion on the polymer surface by promising electrical conductivity.

Figure 7 shows the cross-sectional SEM images of the samples described earlier. The cross section of as-sprayed specimens shows the splat morphology, voids, defects, and interface boundaries between the particle–particle and particle–substrate interfaces (see Fig. 7(*a*)). As the co-ED time increases, the deposition thickness increases as well. At 24 h of deposition, the average thickness

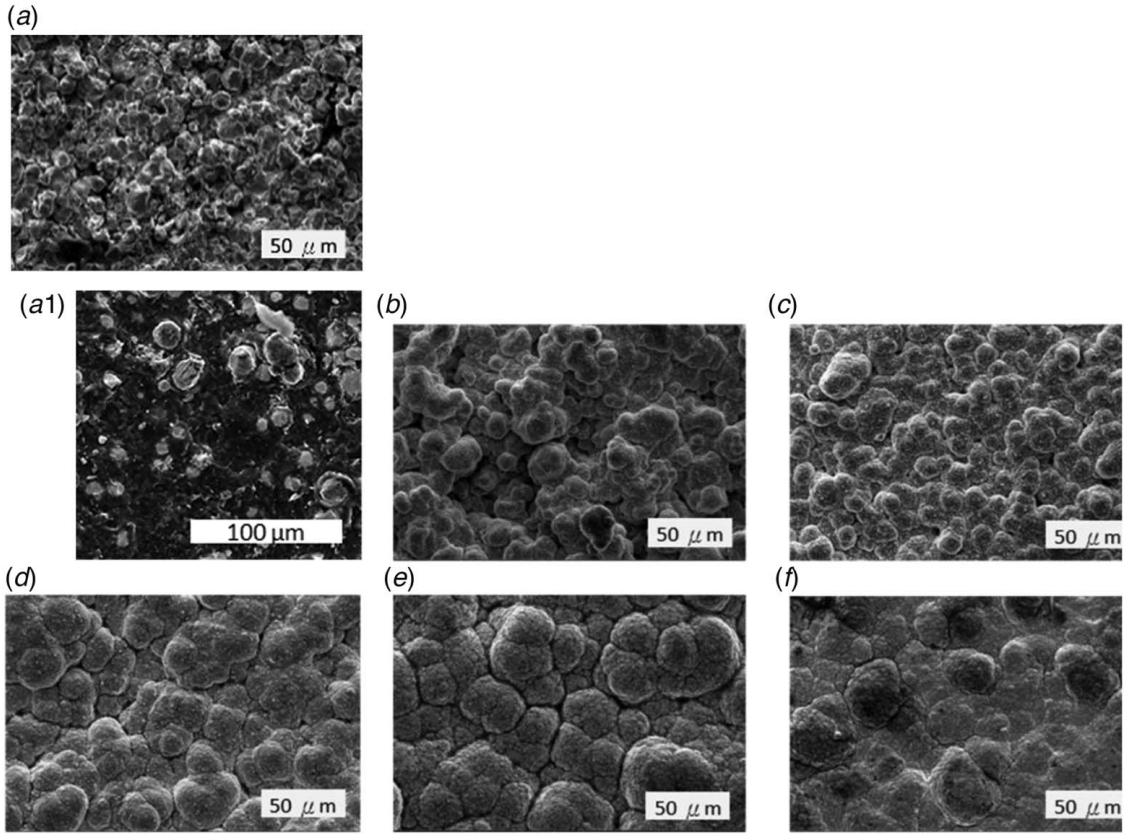

Fig. 6 Surface morpology of (*a*) as-sprayed, (*a*-1) embedded as-sprayed particles onto/into polymer surface, and (*b*) 2 h, (*c*) 4 h, (*d*) 8 h, (*e*) 16, and (*f*) 24 h electroless over-plated samples

reaches up to 100 μm, forming a bulk conductive layer. Electroless deposition created a continuous metallized layer having a high electrical conductivity that could not be solely achieved by the cold-spraying process. As stated in Sec. 1, erosion and locally melting of the polymer under a high-impact bombardment of particles during cold spraying are mainly responsible for the absence of electrical conductivity for as-sprayed (not plated) samples. After introducing a subsequent electroless deposition on the as-cold sprayed layer, high electrical conductivity was selectively achieved on the insulator polymer surface by utilizing a precold-sprayed layer as the catalyst side. Table 5 compares our hybrid coating approach against the studies on solely cold-spray-based polymer metallization reported in the literature. As observed in Table 5, our hybrid approach provides excellent electrical conductivity and comparable adhesion strength versus purely cold spray-based metallization.

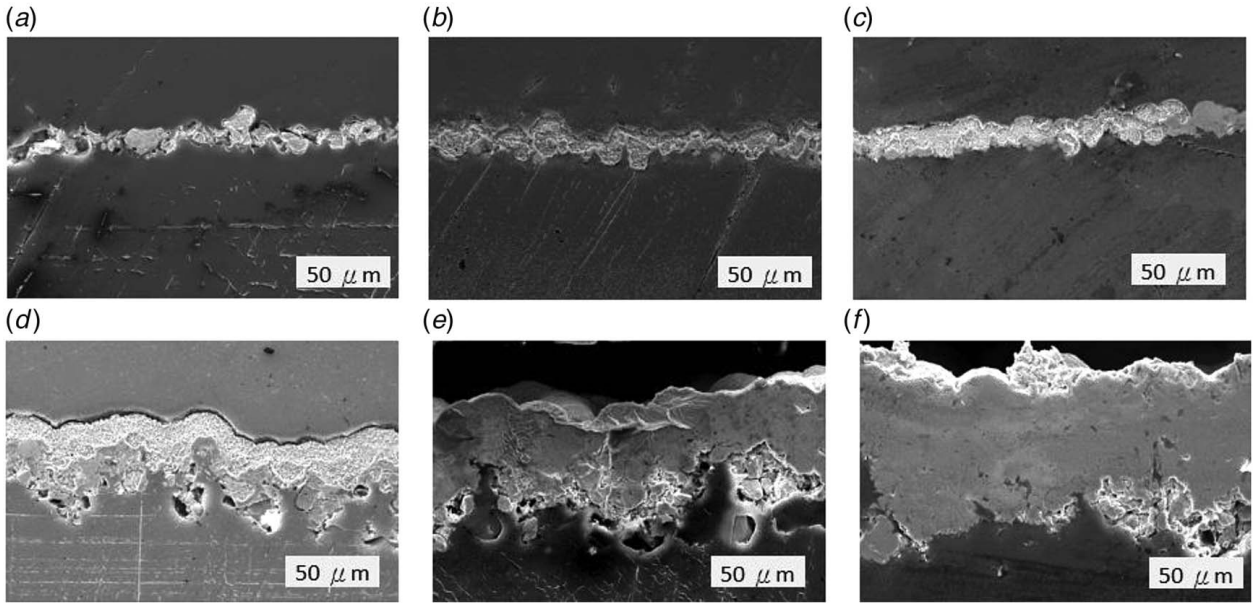

Fig. 7 Cross-sectional SEM images of (*a*) as-sprayed and (*b*) 2 h, (*c*) 4 h, (*d*) 8 h, (*e*) 16, and (*f*) 24 h electroless-plated samples

Table 5 Comparison of electrical conductivity and adhesion performance of CS metallized polymers in the literature

Reference	Substrate material	Feedstock powder	Overplating time (h)	Coating thickness (μm)	Electrical conductivity (MS/m)	Adhesion strength (MPa)	Adhesion test standard
As-cold sprayed (no plating)[a]	Nylon 6	Cu	0 (no plating)	8–10	No conductivity	9.85–10.55	ASTM C-633
CS + 4 h over-plating[a]	Nylon 6	Cu	4	10–15	0.19	6.69–8.31	ASTM C-633
CS + 16 h over-plating[a]	Nylon 6	Cu	16	33–50	4.63	3.66–5.96	ASTM C-633
Gillet et al. [7]	PEEK	Cu	0	100–300	0.02	NA	NA
Bortolussi et al. [36]	CFRP	Cu-PEEK	0	360–780	0.0015	NA	NA
Zhou et al. [8]	CFRP-PEEK	Al/Cu	0	500–200	NA	2.26	PRC GB/T8622
Małachowska et al. [18]	Nylon 6	Cu, Sn + Al	0	0–50	3.8	3.6	DIN EN 582
Che et al. [37]	CFRP	Sn, Cu, Al	0	NA	NA	2.2–7.6	ASTM C-633
Rokni et al. [38]	CFRP-PEEK	Al	0	800–2700	NA	9–18	ASTM D4541

Note: NA denotes "not applicable."
[a]Denotes present study.

3.3 Adhesion Testing. The adhesion tests of the samples was characterized based on the ASTM C633 standard adhesion test [33]. An epoxy-based adhesive (BYK-Gardner 0032, Resin Systems Corp., Amherst, NH) was applied to the interface of the bare polyamide and as-cold-sprayed and also over-plated samples (see Fig. 8(*a*)) according to the ASTM C633 standard. The quantity of the adhesive (glue) and the applied load was carefully controlled during the curing of the adhesive bond. A 22 KIP hydraulic MTS 810 load frame was used in both the adhesion and the tensile tests. The crosshead displacement rate was set to 1 mm/min according to the ASTM D3039 [34]. The adhesive strength of the substrate–coating interface was measured by attaching the substrate/coating specimen to the caps (fixtures) followed by applying a tensile force to the fixtures to detach substrate/coating under exerted force (see Fig. 8(*a*)). The substrate/coating can display either a cohesive fracture with crack propagating through the coating layer or an adhesive fracture at the substrate–coating interface. The test results are disregarded if the substrate/coating disbands from the caps.

Adhesion test was conducted on as-sprayed and electroless-plated specimens considering three specimens for each test. After testing, each set of test results was averaged as shown in Table 5. The adhesion strength of as-sprayed specimens showed the highest adhesion strength while the adhesion strength decreased with increasing co-ED time with larger over-plating thickness. This result is comparable with other studies [35], in which adhesion strength decreases as the coating thickness increases. The adhesion test suggested that the specimens should have a flat surface between the connections of the coated surface to achieve accurate results. However, cold-spray-based particle deposition leads to a certain surface coating roughness, which might influence the results of the adhesion strength. According to surface roughness measurement results, as-cold sprayed samples in this study have a roughness average (R_a) of 1.93 μm, while the plated samples have 6.12 μm and 6.58 μm, after 4 h and 16 h of over-plating, respectively.

For all the as-sprayed and 4-h over-plated specimens, the failure occurs between the epoxy and the polyamide 6 sides. However, for the 16 h specimens, an adhesion failure occurs between the metal and the epoxy (i.e., half of the coated Cu metal attached to the epoxy while the other half is on the polyamide side). As the co-ED plating thickness increased, the failure mode switched from adhesion (between the polymer and metal) to cohesion (within the metal film). The results indicate that the adhesion performance of the as-cold sprayed samples is stronger than the co-ED samples. Although thicker films can be mechanically weaker than thinner films, and so the upper bound in the adhesion strength will be the mechanical interlocked structure, continued

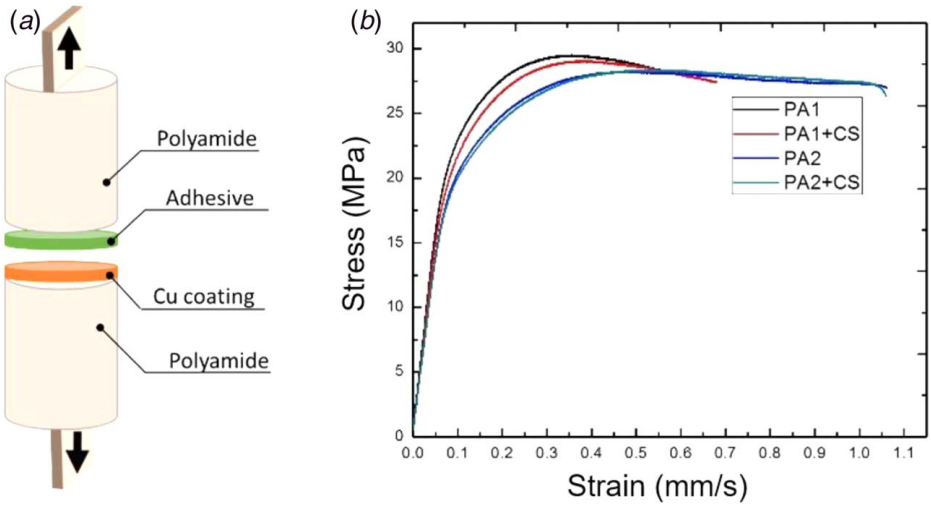

Fig. 8 (*a*) Schematic of the pull-off adhesion test and (*b*) stress–strain (tensile test) results of bulk and as-cold sprayed polyamide 6 polymers

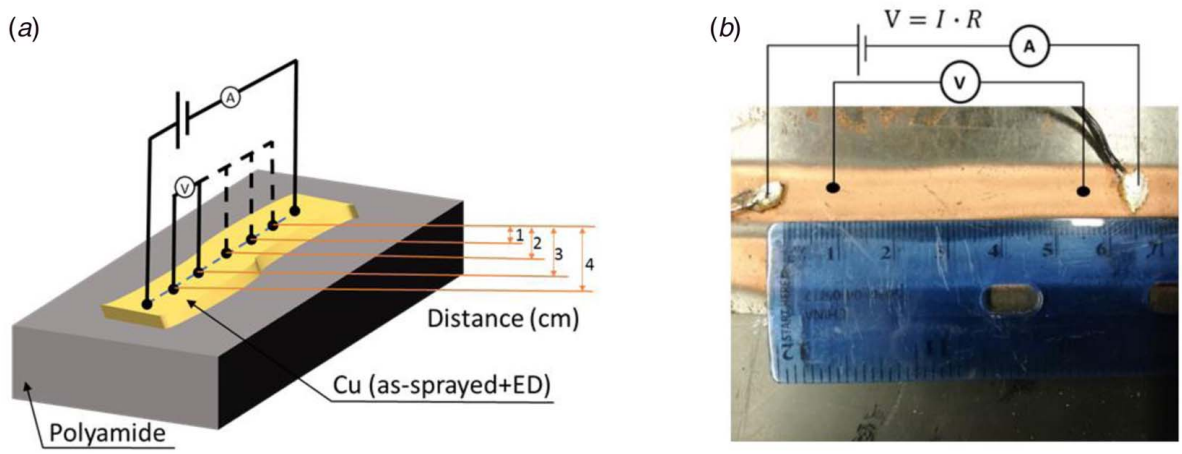

Fig. 9 Four-point probe measurement: (*a*) a schematic of setup and (*b*) experimental setup

metallization of a softer electroless coating slightly degrades the overall system strength, but still to a range that meets or exceeds many published results in Table 5.

3.4 Mechanical Strength (Tensile Test). The tensile test, as shown in Fig. 8(*b*), was conducted on as-sprayed specimens to verify the strength of the resultant coatings. The six dog-bone-shaped [34] polyamide samples having a thickness of 0.2 mm specimens were manufactured. The polyamide specimens labeled as PA1 and PA2 denote the unsprayed specimens, while the PA1 + CS and PA2 + CS present the as-cold-sprayed specimens to compare the sprayed and the unsprayed specimens. One-pass of cold spraying was conducted for the sprayed specimens, keeping some regions intentionally not coated with Cu particles to observe if the un-coated area may influence the tensile strength. The results show that the coated specimens retained their tensile strength compared with the uncoated coupons (see Fig. 8(*b*)). No significant increase or deterioration of tensile strength was observed within the sprayed specimens. As such, the erosion on the polymer surface after the CS process is not severe in terms of mechanical strength. It should be noted that these results are valid under the CS parameters used in the present study.

3.5 Electrical Conductivity. A four-point probes apparatus were used to measure the volume resistivity (i.e., electrical resistivity). As shown in Figs. 9(*a*) and 9(*b*), the four-point probes are designed in which the outer two probes measure the current and the inner two probes measure the voltage. Several coated distances were measured to determine the volume resistivity per-cross-sectional area using the following equation:

$$R = \rho \frac{\ell}{A} \tag{5}$$

where R is the electrical resistance of the coating layer on the substrate calculated from the measured current and voltage, ρ is the electrical volume resistivity, ℓ is the length of the specimen, and A is the cross-sectional area of the coating.

The four-point probe method was measured on all the coated specimens. The as-cold sprayed specimen showed no electrical conductivity, which is likely attributed to surface microstructure, roughness, voids, and defects caused by high-velocity impact of cold sprayed particles on the soft nature polymer surface [39–41]. The measured electrical resistivity ranges from 5.3×10^{-6} (Ω m) to 2.16×10^{-7} (Ω m) for the co-ED specimens of 4 h and 24 h, respectively. The electrical resistivity value is one magnitude lower than the bulk copper resistivity (i.e., $\cong 1.68 \times 10^{-8}$ Ω m) for 16 h over-plated sample. Overall, the resultant coating has high-electrical conductivity between the measurement range of graphite to Cu electrical resistivity. Additionally, the comparison of our hybrid coating approach against the CS coatings in the literature is presented in Table 5. As can be observed, even for smaller coating thickness, the electrical conductivity of the present approach is higher as compared to solely cold spray metallized polymers in the literature, which proves the high fidelity of the electrodes in terms of electrical conductivity. Taken together, the results suggest that hybridizing of CS with a subsequent co-electroless deposition (i.e., overplating) ensures highly-electrically conductive layers on the polymer surfaces, which can be potentially tailored for polymer electronics applications.

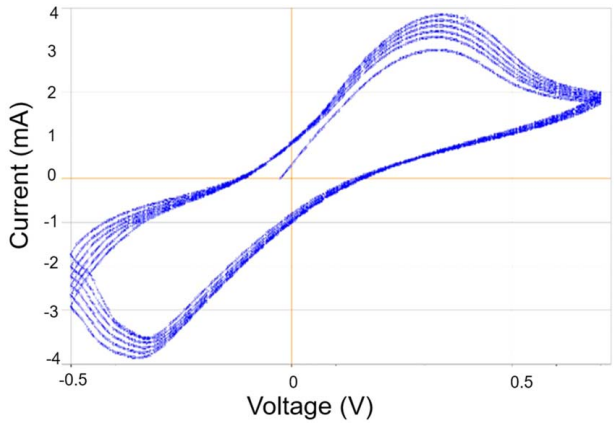

Fig. 10 Cylic voltammetry test results of the 24 h over-plated specimen

Lastly, the electrochemical measurement was performed by cyclic voltammetry (CV) experiments using an apparatus of SP-300 Biologics equipped with the EC-Lab software. All the as-sprayed and electroless deposition specimens were cleaned with DI water to avoid the chemical residual prior to CV experiments. The voltammetry cycle for E was set from 3.5 to −4 (V) at a constant scanning rate of 80 mV/s. The behavior of Cu and CuO in 0.4 M KOH was then examined. The 24 h of electroless deposition specimen was used to conduct a cyclic voltammetry test using the over-coated specimen as the working electrode in the experiments. In Fig. 10, the x-axis represents the applied potential E, while the y-axis represents the current response. The reduction and oxidation curves were cycled five times to confirm the stability. The CV results demonstrated a potential tool to probe reactions between electron transfers of the resulting electrode (i.e., 24-h co-ED sample), indicating excellent electrode stability.

4 Conclusion

Polyimide (Nylon 6) substrate surface was metallized using cold spray particle (Cu) deposition and further over-plated by a subsequent electroless plating process. Finite element analysis was conducted to simulate the morphology changes of Cu particles and polymer substrate deformation upon impact of the particles on the substrate. A viscoelastic model was implemented to the substrate in order to capture the Cu impact responses onto/into the polymer. It was observed that Cu particles were mechanically interlocked into the polymer substrate under described cold spray operating parameters. The results also show that particles' plastic deformation, rebound velocity, and kinetic energy increase with an increasing impact velocity. Conversely, the particle's kinetic energy decreases when the rebound velocity increases. The as-sprayed specimens retained their intrinsic tensile strength even after high-velocity impact during cold spraying. High-electrically conductive functional coatings were achieved on dielectric polymer surface by hybridizing cold spraying with asubsequent over-plating process. The surface and the cross-sectional morphology analyses provided useful information for both the cold-spraying and over-plating processes. The adhesion test revealed that adhesion strength decreases as the thickness of the coating layer increases with a longer over-plating time. Cyclic voltammetry results proved the electrochemical stability of the resultant electrodes. The results uncovered the process-structure properties of cold-spraying and co-electroless overplating processes, which can pave the way for sustainable electronics applications.

Acknowledgment

The authors acknowledge Xingyu Fu and Ziyuan Cheng for their help with sample preparation. The authors also gratefully acknowledge the Purdue University EPICS program. Semih Akin acknowledges a scholarship support through the Office of Overseas Scholarship Program from the Republic of Turkey Ministry of National Education.

Conflict of Interest

There are no conflicts of interest. This article does not include research in which human participants were involved. Informed consent is not applicable. This article does not include any research in which animal participants were involved.

Data Availability Statement

The data sets generated and supporting the findings of this article are obtainable from the corresponding author upon reasonable request.

References

[1] Tsai, J. T., Lin, L. K., Lin, S. T., Stanciu, L., and Jun, M. B. G., 2021, "Influence of Bi_2O_3 Glass Powder in the Silver Paste and the Impact on Silicon Solar Cell Substrates," Mater. Des., **200**.

[2] Lin, L. K., Tsai, J. T., Díaz-Amaya, S., Oduncu, M. R., Zhang, Y., Huang, P. Y., Ostos, C., et al.et al., 2021, "Antidelaminating, Thermally Stable, and Cost-Effective Flexible Kapton Platforms for Nitrate Sensors, Mercury Aptasensors, Protein Sensors, and p-Type Organic Thin-Film Transistors," ACS Appl. Mater. Interfaces, **13**(9), pp. 11369–11384.

[3] Akin, S., Gabor, T., Jo, S., Joe, H., Tsai, J.-T., Park, Y., Lee, C. H., Park, M. S., and Jun, M. B.-G., 2020, "Dual Regime Spray Deposition Based Laser Direct Writing of Metal Patterns on Polymer Substrates," ASME J. Micro-Nano-Manuf., **8**(2), p. 024511.

[4] Wang, M., Wang, X., Moni, P., Liu, A., Han Kim, D., Jun Jo, W., Sojoudi, H., et al., 2017, "CVD Polymers for Devices and Device Fabrication," Adv. Mater., **29**(11), p. 1604606.

[5] Liu, X., Gong, P., Hu, H., Zhao, M., Zhang, K., and Zhou, H., 2021, "Study on the Tribological Properties of PVD Polymer-Like Carbon Films in Air/Vacuum/N2and Cycling Environments," Surf. Coatings Technol., **406**.

[6] Lupoi, R., and O'Neill, W., 2010, "Deposition of Metallic Coatings on Polymer Surfaces Using Cold Spray," Surf. Coatings Technol., **205**(7), pp. 2167–2173.

[7] Gillet, V., Aubignat, E., Costil, S., Courant, B., Langlade, C., Casari, P., Knapp, W., and Planche, M. P., 2019, "Development of Low Pressure Cold Sprayed Copper Coatings on Carbon Fiber Reinforced Polymer (CFRP)," Surf. Coatings Technol., **364**, pp. 306–316.

[8] Zhou, X. L., Chen, A. F., Liu, J. C., Wu, X. K., and Zhang, J. S., 2011, "Preparation of metallic coatings on polymer matrix composites by cold spray," Surf. Coatings Technol., **206**(1), pp. 132–136.

[9] Che, H., Vo, P., and Yue, S., 2019, "Investigation of Cold Spray on Polymers by Single Particle Impact Experiments," J. Therm. Spray Technol., **28**(1–2), pp. 135–143.

[10] Della Gatta, R., Perna, A. S., Viscusi, A., Pasquino, G., and Astarita, A., 2021, "Cold Spray Deposition of Metallic Coatings on Polymers: A Review," J. Mater. Sci., **57**(1), pp. 27–57.

[11] Parmar, H., Tucci, F., Carlone, P., and Sudarshan, T. S., 2021, "Metallisation of Polymers and Polymer Matrix Composites by Cold Spray: State of the Art and Research Perspectives," Int. Mater. Rev., pp. 1–25.

[12] Yin, S., Cavaliere, P., Aldwell, B., Jenkins, R., Liao, H., Li, W., and Lupoi, R., 2018, "Cold Spray Additive Manufacturing and Repair: Fundamentals and Applications," Addit. Manuf., **21**, pp. 628–650.

[13] Xie, Y., Chen, C., Planche, M. P., Deng, S., Huang, R., Ren, Z., and Liao, H., 2019, "Strengthened Peening Effect on Metallurgical Bonding Formation in Cold Spray Additive Manufacturing," J. Therm. Spray Technol., **28**(4), pp. 769–779.

[14] Melentiev, R., Yu, N., and Lubineau, G., 2021, "Polymer Metallization via Cold Spray Additive Manufacturing: A Review of Process Control, Coating Qualities, and Prospective Applications," Addit. Manuf., **48**(Part B). . Article Number:102459.

[15] Che, H., Chu, X., Vo, P., and Yue, S., 2018, "Metallization of Various Polymers by Cold Spray," J. Therm. Spray Technol., **27**(1–2), pp. 169–178.

[16] King, P. C., Poole, A. J., Horne, S., de Nys, R., Gulizia, S., and Jahedi, M. Z., 2013, "Embedment of Copper Particles Into Polymers by Cold Spray," Surf. Coatings Technol., **216**, pp. 60–67.

[17] Ganesan, A., Affi, J., Yamada, M., and Fukumoto, M., 2012, "Bonding Behavior Studies of Cold Sprayed Copper Coating on the PVC Polymer Substrate," Surf. Coatings Technol., **207**, pp. 262–269.

[18] Małachowska, A., Winnicki, M., Konat, Ł, Piwowarczyk, T., Pawłowski, L., Ambroziak, A., and Stachowicz, M., 2017, "Possibility of Spraying of Copper Coatings on Polyamide 6 With Low Pressure Cold Spray Method," Surf. Coatings Technol., **318**, pp. 82–89.

[19] Akin, S., Tsai, J.-T., Park, M. S., Jeong, Y. H., and Jun, M., 2021, "Fabrication of Electrically Conductive Patterns on ABS Polymer Using Low-Pressure Cold Spray and Electroless Plating," ASME J. Micro- Nano-Manuf., **8**(4), p. 041014.

[20] Fallah, P., Rajagopalan, S., McDonald, A., and Yue, S., 2020, "Development of Hybrid Metallic Coatings on Carbon Fiber-Reinforced Polymers (CFRPs) by Cold Spray Deposition of Copper-Assisted Copper Electroplating Process," Surf. Coatings Technol., **400**.

[21] Equbal, A., Equbal, A., and Sood, A. K., 2014, "Metallization on FDM Processed Parts Using Electroless Procedure," Procedia Mater. Sci., **6**, pp. 1197–1206.

[22] Sahoo, S. K., Sahu, A. K., and Mahapatra, S. S., 2017, "Environmental Friendly Electroless Copper Metallization on FDM Build ABS Parts," Int. J. Plast. Technol., **21**(2), pp. 297–312.

[23] Olivera, S., Muralidhara, H. B., Venkatesh, K., Gopalakrishna, K., and Vivek, C. S., 2016, "Plating on Acrylonitrile–Butadiene–Styrene (ABS) Plastic: A Review," J. Mater. Sci., **51**(8), pp. 3657–3674.

[24] Delloro, F., Jeandin, M., Jeulin, D., Proudhon, H., Faessel, M., Bianchi, L., Meillot, E., and Helfen, L., 2017, "A Morphological Approach to the Modeling of the Cold Spray Process," J. Therm. Spray Technol., **26**(8), pp. 1838–1850.

[25] Dykhuizen, R. C., Smith, M. F., Gilmore, D. L., Neiser, R. A., Jiang, X., and Sampath, S., 1999, "Impact of High Velocity Cold Spray Particles," J. Therm. Spray Technol., **8**(4), pp. 559–564.

[26] Assadi, H., Kreye, H., Gärtner, F., and Klassen, T., 2016, "Cold Spraying – A Materials Perspective," Acta Mater., **116**, pp. 382–407.

[27] Bergström, J. S., Bowden, A. E., Rimnac, C. M., and Kurtz, S. M., 2012, "Development and Implementation of an Advanced User Material Model for UHMWPE," Proceedings of the Ninth International LS-DYNA Users Conference, Detroit, MI, June 3–5.

[28] Tsai, J.-T., Akin, S., Zhou, F., Bahr, D. F., and Jun, M. B.-G., 2021, "Establishing a Cold Spray Particle Deposition Window on Polymer Substrate," J. Therm. Spray Technol., **30**(4), pp. 1069–1080.

[29] Bergstrom, J. S., and Bischoff, J. E., 2010, "An Advanced Thermomechanical Constitutive Model for UHMWPE," Int. J. Struct. Changes Solids, **2**(1), pp. 31–39.

[30] Bergström, J. S., and Boyce, M. C., 2000, "Deformation of Elastomeric Networks: Relation Between Molecular Level Deformation and Classical Statistical Mechanics Models of Rubber Elasticity," Macromolecules, **34**(3), pp. 614–626.

[31] Pouriayevali, H., 2013, Describing Large Deformation of Polymers at Quasi-Static and High Strain Rate.

[32] Jo, S., Akin, S., Park, M. S., and Jun, M. B. G., 2021, "Selective Metallization on Glass Surface by Laser Direct Writing Combined With Supersonic Particle Deposition," Manuf. Lett.

[33] ASTM International, 2001, *ASTM C633 – Standard Test Method for Adhesion or Cohesion Strength of Thermal Spray Coatings*, Vol. 02, ASTM, West Conshohocken, PA. https://www.astm.org/c0633-01.html

[34] ASTM International, 2017, *ASTM D3039/D3039M-14 Standard Test Method for Tensile Properties of Polymer Matrix Composite Materials*, Vol. 15, ASTM, West Conshohocken, PA. https://www.astm.org/d3039_d3039m-14.html
[35] Leterrier, Y., Boogh, L., Andersons, J., and Månson, J.-A. E., 1997, "Adhesion of Silicon Oxide Layers on Poly (Ethylene Terephthalate). I: Effect of Substrate Properties on Coating's Fragmentation Process," J. Polym. Sci., Part B: Polym. Phys., **35**(9), pp. 1463–1472.
[36] Bortolussi, V., Borit, F., Chesnaud, A., Jeandin, M., Faessel, M., Figliuzzi, B., Willot, F., Roche, K., and Surdon, G., 2016, "Cold Spray of Metal-Polymer Composite Coatings Onto Carbon Fiber-Reinforced Polymer (CFRP)," International Thermal Spray Conference 2016 (ITSC), Shanghai/China.
[37] Che, H., Vo, P., and Yue, S., 2017, "Metallization of Carbon Fibre Reinforced Polymers by Cold Spray," Surf. Coatings Technol., **313**, pp. 236–247.
[38] Rokni, M. R., Feng, P., Widener, C. A., and Nutt, S. R., 2019, "Depositing Al-Based Metallic Coatings Onto Polymer Substrates by Cold Spray," J. Therm. Spray Technol., **28**(7), pp. 1699–1708.
[39] Gonzalez, R., Ashrafizadeh, H., Lopera, A., Mertiny, P., and McDonald, A., 2016, "A Review of Thermal Spray Metallization of Polymer-Based Structures," J. Therm. Spray Technol., **25**(5), pp. 897–919.
[40] Bortolussi, V., Figliuzzi, B., Willot, F., Faessel, M., and Jeandin, M., 2018, "Morphological Modeling of Cold Spray Coatings," Image Anal. Stereol., **37**(2), pp. 145–158.
[41] Bortolussi, V., Figliuzzi, B., Willot, F., Faessel, M., and Jeandin, M., 2020, "Electrical Conductivity of Metal–Polymer Cold Spray Composite Coatings Onto Carbon Fiber-Reinforced Polymer," J. Therm. Spray Technol., **29**(4), pp. 642–656.